ORGANIC CHEMISTRY FRONTIERS

RESEARCH ARTICLE

View Article Online
View Journal | View Issue

Cite this: *Org. Chem. Front.*, 2023, **10**, 1903

A BODIPY-based probe for amyloid-β imaging *in vivo*†

Mingguang Zhu,[a] Guoyang Zhang,[a] Ziwei Hu,[a] Chaofeng Zhu,[a] Yixiang Chen,[a] Tony D. James, *[b,c] Lijun Ma*[a] and Zhuo Wang *[a,b]

Received 29th December 2022,
Accepted 8th March 2023

DOI: 10.1039/d2qo02032g

rsc.li/frontiers-organic

Alzheimer's disease (AD) is a neurodegenerative disease, and the efficient detection of amyloid-β (Aβ) plaques can greatly enhance diagnosis and therapy. Most reported probes used to detect Aβ are based on the *N*,*N*-dimethylamino group. As such, the design of new Aβ-recognition units facilitates the recognition of Aβ. Herein, we present an Aβ recognition unit [4-(Boc-amino) benzene] used to develop BocBDP. BocBDP can recognize and image Aβ plaques both *in vitro* and *in vivo* through the interaction with amino acid residues Lys16 (K16), Val18 (V18), and Glu22 (E22). The hydrogen bonding interaction (1.9 Å) between the carbonyl oxygen atom in the Boc unit and the amino acid residue K16 allows BocBDP to bind strongly to Aβ, resulting in a five-fold fluorescence enhancement and a high affinity (K_d = 67.8 ± 3.18 nM). BocBDP can cross the BBB and image Aβ for at least 2 hours. We anticipate that our Aβ recognition unit will help improve the design of probes that specifically recognize Aβ.

Introduction

Alzheimer's disease (AD) is a neurodegenerative disease with complex pathogenesis that seriously affects human health.[1] On the basis of the amyloid cascade hypothesis, amyloid-β (Aβ) is formed by the hydrolysis of the amyloid precursor protein (APP), and the deposition of Aβ in the brain is responsible for AD.[2,3] Aβ has different subtypes, such as soluble monomers, dimers, oligomers, insoluble protofibrils and fibril plaques.[4,5] The continuous deposition of Aβ gradually affects the normal physiological function of neurons, eventually leading to irreversible brain dysfunction.[6,7] Therefore, selective imaging of Aβ is helpful for the early diagnosis of AD.

The blood–brain barrier (BBB) is an important protective barrier for the brain. The BBB is closely connected by brain capillary endothelial cells (BCECS), pericytes, astrocytes, and neuronal cells.[8,9] The BBB can protect the brain from damage caused by harmful substances in the blood and maintain the stability of the internal environment of the brain. The BBB blocks almost 100% of macromolecules and more than 98% of organic small molecules entering the brain.[10] However, the protective mechanism poses difficulties for the development of drugs and probes for treating and imaging the brain.[11] Due to the existence of the BBB, the imaging and diagnosis of Aβ *in vivo* are difficult.

Currently, many diagnostic techniques have been used to reveal pathologic changes in AD patients, such as single photon emission computed tomography (SPECT), positron emission tomography (PET), and magnetic resonance imaging (MRI).[12–14] Compared with these methods, fluorescence imaging has the advantages of high sensitivity, high resolution, low cost, and non-invasiveness and as such is a promising method for the diagnosis of AD.[15–21]

For the detection of Aβ plaques, chemical probes with high selectivity and binding affinity for Aβ are required. For imaging Aβ *in vivo*, the probes should have a suitable oil–water partition coefficient ($2 < \log P < 5$) and molecular weight (MW < 500 Da) to guarantee satisfactory BBB penetration. Therefore, probes that meet these requirements easily cross the BBB and facilitate Aβ imaging *in vivo*.[22–26] Thioflavin-T (ThT) is the gold standard probe for imaging Aβ plaques. ThT has a rotatable single bond between *N*,*N*-dimethylaniline and thiazole quaternary ammonium salt. As such, ThT is a typical intramolecular charge transfer (ICT) probe with a molecular rotor structure. However, the application of ThT *in vivo* has been hindered because of restricted BBB penetration and a short emission wavelength.[27] To date, most reported probes for the detection of Aβ plaques are based on a donor–π–acceptor structure. The *N*,*N*-dimethylamino group is a typical electron-donating group,

[a]*State Key Laboratory of Chemical Resource Engineering, College of Chemistry, Beijing Advanced Innovation Center for Soft Matter Science and Engineering, Beijing University of Chemical Technology, Beijing 100029, China.*
E-mail: wangzhuo77@mail.buct.edu.cn, lijun_ma@foxmail.com;
Fax: +86-01-64434898
[b]*Department of Chemistry, University of Bath, Bath BA2 7AY, UK.*
E-mail: T.D.James@bath.ac.uk
[c]*School of Chemistry and Chemical Engineering, Henan Normal University, Xinxiang 453007, China*

†Electronic supplementary information (ESI) available. See DOI: https://doi.org/10.1039/d2qo02032g

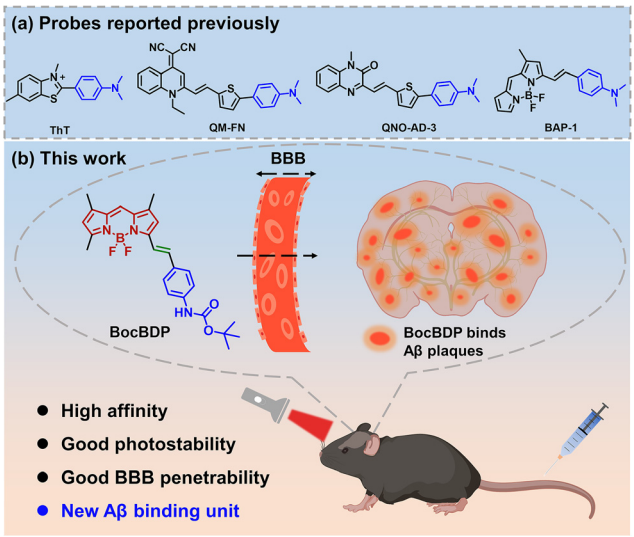

Fig. 1 (a) Previously reported probes for the detection of Aβ aggregates. (b) Probe BocBDP with a binding unit suitable for penetrating the BBB and imaging Aβ *in vivo*.

which can interact with the hydrophobic cavities of Aβ aggregates and can be used to recognize Aβ (Fig. 1a and Table S1†).[28–30] Although many Aβ probes have been reported to date, improved binding units for imaging Aβ selectively are still required. Herein, we developed a probe BocBDP to recognize and image Aβ both *in vitro* and *in vivo*. BocBDP consists of a *tert*-butoxycarbonyl (Boc) modified aniline unit and a BODIPY unit, which are conjugated by a π-bridge (Fig. 1b). The Boc-modified aniline unit serves as both an electron-donating group and an Aβ recognition unit, while the BODIPY unit serves as the fluorophore. The new probe has a high affinity (K_d = 67.8 ± 3.18 nM) for Aβ and the ability to cross the BBB to image Aβ *in vivo* (Fig. 1b).

Results and discussion

Design, theoretical calculations, and synthesis of the probe

The free rotation of the *N*,*N*-dimethylamino group facilitates changes in the fluorescence spectra or emission intensity, when the probe binds to the amino acid residues in hydrophobic cavities.[31,32] Since no hydrogen bond forms between the *N*,*N*-dimethylamino group and these amino acid residues, the probe is only weakly bound to Aβ and is rapidly metabolized. Hydrogen bonding can result in stronger binding of the probe to Aβ. As such, the introduction of hydrogen bonding sites into probes can enhance the binding with Aβ and facilitate extended imaging. However, the introduction of hydrogen bonds to enhance protein–probe interactions often results in no net increase of binding affinity (K_d).[33–35] Nevertheless, hydrogen bonding plays a significant role in the recognition of biological molecules.[36] Specifically, the intermolecular hydrogen bonding between proteins and organic ligands involves N, O, S and halogen atoms. The hydrogen bond length of NH···O (3.04 Å) is shorter than that of NH···N (3.10 Å).[37] Therefore, the introduction of an oxygen atom can reduce the distance between the probe and the protein, thus enhancing the hydrogen bonding interactions. BAP-1 is a molecular rotor based fluorescent probe. The free rotation of the *N*,*N*-dimethylamino group of BAP-1 can induce non-radiative transitions between the HOMO and LUMO, resulting in low fluorescence intensity. However, the introduction of oxygen atoms can affect the free rotation of the amino group, which may increase the fluorescence intensity of the probes. So, the introduction of an additional freely rotating group such as the *tert*-butyl group is required to balance the enhanced hydrogen bonding and ensure that the fluorescence intensity remains low. *tert*-Butoxycarbonyl (Boc) has two oxygen atoms and the *tert*-butyl group of Boc can also rotate freely (Fig. 1b). Conjugation of the carbonyl with the oxygen of the Boc group makes the carbonyl oxygen atom more negatively charged, facilitating the interaction of the oxygen lone pair electrons with the NH residues through hydrogen bonding. Therefore, with this research, the Boc group was introduced to develop a probe we called BocBDP for sensing Aβ instead of the *N*,*N*-dimethylamino group. BocBDP was linked by Boc-modified aniline [4-(Boc-amino) benzene] to a BODIPY core using a double bond (Fig. 1b).

BocBDP is structurally composed of an electron-donating group 4-(Boc-amino) benzene and an electron-withdrawing group BODIPY. The two groups are conjugated and connected by a π-bridge. The donor–acceptor architecture allows BocBDP to exhibit ICT properties. To predict whether BocBDP exhibits an ICT effect, Gaussian calculations were performed using density functional theory (DFT) methods using B3LYP/6-311+(d,p). As shown in Fig. 2a, the electron cloud in the highest occupied molecular orbital (HOMO) was distributed

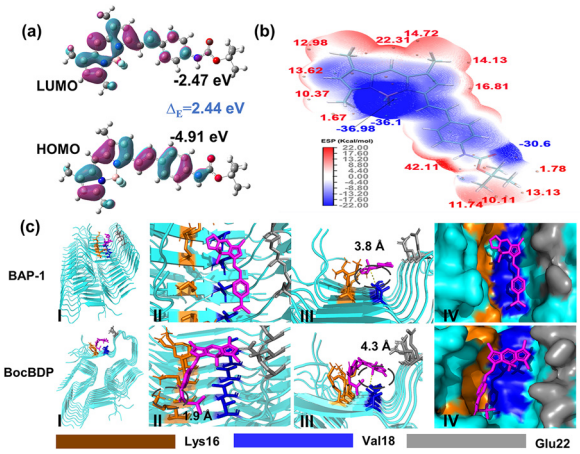

Fig. 2 Theoretical calculations and molecular docking results. (a) The highest occupied molecular orbital (HOMO) and the lowest unoccupied molecular orbital (LUMO) of BocBDP. (b) The surface electrostatic potential of BocBDP. (c) The docking results of BAP-1 and BocBDP. (I) The global view of molecular docking. (II) Licorice form of the molecule in the $A\beta_{1-42}$ aggregate model. (III) The average distance between the probe and the amino acid residues of the pocket. (IV) Molecular surface form of the molecule in the $A\beta_{1-42}$ aggregate model.

along the conjugate unit of BocBDP. The electron cloud in the lowest unoccupied molecular orbital (LUMO) was mainly distributed on the BODIPY backbone. The obtained electron distribution was redistributed from 4-(Boc-amino) benzene in the HOMO to the BODIPY backbone in the LUMO. The energy gap (ΔE) of BocBDP was 2.44 eV (Fig. 2a). The change of the electron cloud and the small ΔE value confirms the presence of ICT. The surface electrostatic potential of BocBDP and the distribution area were calculated using Multiwfn software.[38] The negative potential of BocBDP was mainly distributed on BODIPY, while the three methyl groups of Boc exhibited positive potential (Fig. 2b and Fig. S1†). The results indicated that the ester group in the Boc unit and the fluorine atom in BODIPY were electron-withdrawing groups. The introduction of the Boc unit reduced the electron-donating ability of the amino group, thus weakening the ICT effect of BocBDP. As such, the flow of the electron cloud from the HOMO to LUMO was not so significant (Fig. 2a), which causes a reduced ICT effect and a small Stokes shift.

To predict the interaction between BocBDP and $A\beta_{1-42}$ aggregates, we performed molecular docking studies. 5KK3 is one of the popular $A\beta_{1-42}$ aggregate protein models.[39] The fibril core of 5KK3 consists of a dimer of $A\beta_{1-42}$ molecules. Each molecule contains four β-strands in an S-shaped amyloid fold. 5KK3 is arranged to generate two hydrophobic cores that are capped at the end of the chain by a salt bridge. The outer surface of 5KK3 presents hydrophilic side chains to the solvent. 5KK3 provided a sufficient β-sheet structure to predict the interaction between BocBDP and $A\beta_{1-42}$ aggregates. Docking calculations were processed using Autodock Tools 1.5.6, PyMOL, and Python software. The docking results were analysed using PyMOL software. Amino acid residues 16–21 (KLVFFA) are highly hydrophobic and constitute the hydrophobic region of the $A\beta_{1-42}$ aggregates. The peptide fragment $A\beta_{16-21}$ (KLVFFA) is widely accepted as the core structure of $A\beta_{1-42}$ aggregates.[40] So, these amino acid residues provide hydrophobic pockets that enable interaction between BocBDP and $A\beta_{1-42}$ aggregates. As shown in Fig. 2c-I, BAP-1 and BocBDP interact with the same amino residues Lys16 (K16), Val18 (V18), and Glu22 (E22), but they insert into the hydrophobic pockets of Aβ in different directions. BocBDP exhibits a hydrogen bond (1.9 Å) between the carbonyl oxygen atom of the Boc unit and the amino acid residue K16. While no hydrogen bond was found for BAP-1 (Fig. 2c-II). The depth that BocBDP and BAP-1 insert into the hydrophobic pockets was also different. The average distance between BocBDP and the amino acid residues was 4.3 Å, while that between BAP-1 and the amino acid residues was 3.8 Å (Fig. 2c-III). Typically, K_d is related to how deeply the probe inserts into the pocket of the protein. K_d is reduced when the probe is deeply inserted into the pocket. Therefore, the K_d of BocBDP was larger than that of BAP-1 because the depth that BocBDP enters the pocket was less than that for BAP-1. The docking results illustrate that BocBDP exhibits good potential to interact with $A\beta_{1-42}$ aggregates, so we synthesized BocBDP and evaluated its ability for the recognition of $A\beta_{1-42}$ *in vivo*.

The synthetic route to BocBDP is shown in Schemes S1 and S2.† The key step in the formation of the BODIPY backbone (compound **3**) was the condensation of 3,5-dimethylpyrrole-2-carbaldehyde (compound **1**) and 2,4-dimethylpyrrole (compound **2**) at low temperatures, followed by the addition of triethylamine (Et_3N) and boron trifluoride diethyl etherate ($BF_3{\cdot}Et_2O$). BocBDP was successfully prepared by the condensation of BODIPY and 4-(Boc-amino) benzaldehyde in the presence of piperidine and acetic acid, with a yield of 15%. The molecular structures were characterized by nuclear magnetic resonance (NMR) and high-resolution mass spectrometry (HRMS). The detailed data are given in the ESI (Fig. S5–S8†).

Optical properties of BocBDP and its response to Aβ

The optical properties of BocBDP were evaluated in five solvents with different polarities. As shown in Fig. 3a, BocBDP exhibited one strong absorbance band at around 570 nm. With the increase of solvent polarity, the maximum absorption wavelength changed slightly (~14 nm). As shown in Fig. 3b, the fluorescence spectra exhibited a sharp spectral band from 570 to 700 nm. With the increase of solvent polarity, the maximum emission wavelength redshifted slightly (~12 nm). The Stokes shift was 14 nm in DMSO (Table S2†), which confirmed the results from the calculations that BocBDP exhibits

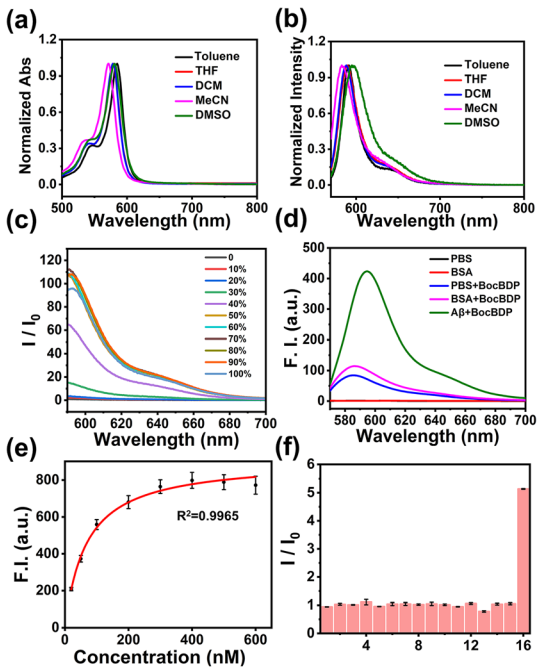

Fig. 3 (a) The normalized absorption spectra of BocBDP (1 μM) in different solvents. (b) The normalized fluorescence spectra of BocBDP (1 μM) in different solvents. (λ_{ex} = 550 nm). (c) The viscosity response characteristics of BocBDP. (d) Fluorescence response of BocBDP (1 μM in PBS) to $A\beta_{1-42}$ aggregates (20 μg mL^{-1} in PBS, final concentration) and BSA (10 μg mL^{-1}, final concentration). (e) Saturated binding assay (K_d) of BocBDP to $A\beta_{1-42}$ aggregates. (f) Interference assays (λ_{em} = 600 nm) for BocBDP (1 μM) and various potential interferents (20 μM). 1–16 refers to Na^+, K^+, Ca^{2+}, Co^{2+}, Cu^{2+}, Zn^{2+}, Mg^{2+}, Fe^{2+}, Fe^{3+}, Al^{3+}, Cys, Phe, Val, GSH, Leu, and $A\beta_{1-42}$ aggregates, respectively.

a weak ICT effect. The fluorescence intensity of the probe is enhanced when the motion of the probe is restricted.[41] Therefore, we evaluated the response of BocBDP to viscosity. The fluorescence intensity of BocBDP was weak in 20% 1,2-propanediol/water (v/v). The fluorescence intensity started to increase in 30% 1,2-propanediol/water (v/v), and increased significantly at 40%, and approached a maximum value at about 70% (Fig. 3c). These results indicated that BocBDP was sensitive to viscosity, and the fluorescence intensity of BocBDP was enhanced when bound with $A\beta_{1-42}$ aggregates. In the following experiments, we prepared $A\beta_{1-42}$ aggregates and evaluated the interaction between BocBDP and $A\beta_{1-42}$ aggregates. The $A\beta_{1-42}$ aggregates formed were characterized using a transmission electron microscope (TEM). It was observed that the morphology of $A\beta_{1-42}$ aggregates was filamentous, indicating that the $A\beta_{1-42}$ aggregates were prepared successfully (Fig. S2†). In Fig. 3d, a five-fold enhancement of fluorescence was observed when BocBDP interacted with $A\beta_{1-42}$ aggregates. In addition, a 9 nm red-shift was observed when BocBDP interacts with $A\beta_{1-42}$ aggregates. These results confirmed that BocBDP was inserted into the hydrophobic pocket of the $A\beta_{1-42}$ aggregates, and the molecular motion of BocBDP was restricted, resulting in an enhanced fluorescence output. Differences in the microenvironment of the hydrophobic pocket cause a red-shifted emission wavelength. The experimental results were consistent with the docking results (Fig. 2c and d). Human serum albumin (HSA) is a major component of blood and is widely distributed in the human body. Bovine serum albumin (BSA) is commonly used as an inexpensive analogue of HSA due to their structural similarity.[42] BSA may cause non-specific fluorescence enhancement of the probe. Therefore, the interaction between BocBDP and BSA was evaluated. When BocBDP interacts with BSA, a slight enhancement was observed, indicating weak non-specific binding (Fig. 3b). The fluorescence response of BocBDP to different interferences was also evaluated. As shown in Fig. 3f, except for $A\beta_{1-42}$ aggregates, the fluorescence intensity was not obviously changed. The results illustrated that BocBDP exhibited good selectivity for $A\beta_{1-42}$ aggregates. To quantify the binding affinity (K_d), fluorescence-based saturation binding assays were conducted. A lower K_d value means a higher affinity. In Fig. 3e and Table S1,† the K_d of BocBDP to $A\beta_{1-42}$ aggregates was 67.8 ± 3.18 nM, which was smaller than those of ThT (K_d = 890 nM), IRI-1 (K_d = 374 nM), RM-28 (K_d = 175.69 nM), and DCIP-1 (K_d = 674.3 nM). The K_d of BocBDP was larger than that of BAP-1(K_d = 44.1 nM), which was consistent with the docking results (Fig. 2c). Although the K_d of BocBDP was larger than that of BAP-1, the K_d value of BocBDP was suitable for practical applications. Meanwhile, we conducted a photostability experiment to determine the stability of BocBDP under light excitation. The fluorescence intensity of BocBDP hardly changed after 300 s (Fig. S3†).

In vitro fluorescence staining

To confirm the binding of BocBDP to $A\beta_{1-42}$ aggregates, fluorescence staining experiments were performed in a solution of $A\beta_{1-42}$ aggregates and the brain slices of AD mice (APP/PS1, 10 months old, female). Pre-prepared $A\beta_{1-42}$ aggregate solution was placed on glass slides and incubated with BocBDP and ThT. $A\beta_{1-42}$ aggregates exhibited plaque-like structures under a confocal laser scanning microscope (CLSM). ThT highlighted $A\beta_{1-42}$ aggregates in green, and BocBDP highlighted $A\beta_{1-42}$ aggregates in red (Fig. 4a and c). The plaque-like structures stained with BocBDP merged well with that of ThT (Fig. 4b and d). The staining results of brain slices of the AD mice correlated well with the $A\beta_{1-42}$ aggregates in solution. BocBDP exhibited a high signal-to-noise ratio for staining Aβ plaques

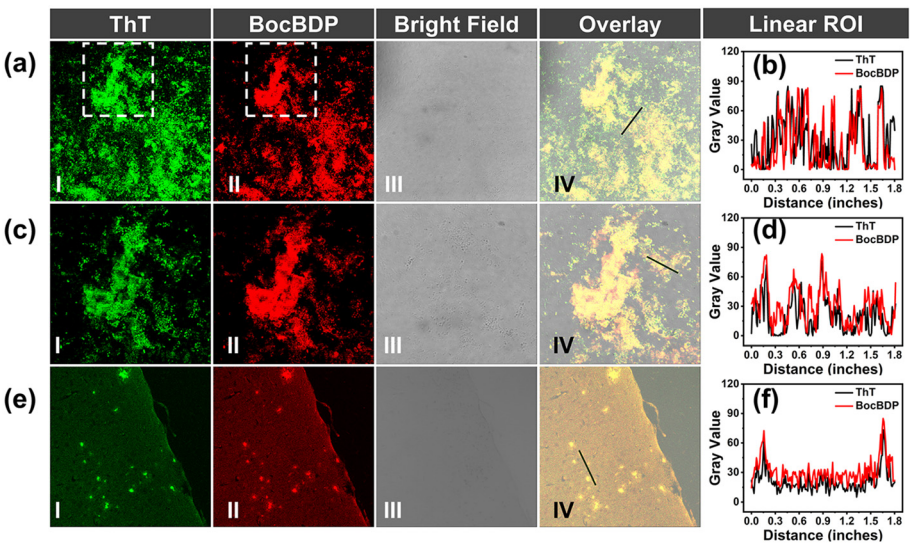

Fig. 4 (a) Images of the $A\beta_{1-42}$ aggregate solution stained with (I) ThT (λ_{ex} = 488 nm) and (II) BocBDP (λ_{ex} = 543 nm), (III) bright-field image, and (IV) merged figures. (c) The enlarged view of the box in figure a. (e) Images of the brain slices stained with (I) ThT (λ_{ex} = 488 nm) and (II) BocBDP (λ_{ex} = 543 nm), (III) bright-field image, and (IV) merged figures. (b, d and f) The intensity profile of linear ROI.

and merged well with those stained with ThT (Fig. 4e). The stained plaques exhibited excellent colocalization with the commercial Aβ probe ThT, suggesting that BocBDP was able to specifically stain Aβ plaques in the AD mice brain tissue (Fig. 4f).

Biocompatibility

Inspired by the fluorescence staining results, the biocompatibility of BocBDP was evaluated with PC12 cells. The cytotoxicity of BocBDP was evaluated by using a standard MTT assay and the results indicated that BocBDP had no significant cytotoxicity, even when the concentration was up to 20 μM (Fig. 5a). The hemolysis rate (HR) was evaluated and it was found that the HR of BocBDP was low (Fig. 5b). These results confirmed that BocBDP exhibits good biocompatibility and was suitable for *in vivo* applications.

In vivo fluorescence imaging

The BBB is an important factor that needs to be considered for *in vivo* imaging. Generally, probes with log *P* between 2 and 5 and MW less than 500 Da cross the BBB and facilitate imaging *in vivo*.[22] The log *P* of BocBDP was calculated as 3.74 and the MW was less than 500 Da (Table S1†). Therefore, BocBDP has the possibility to cross the BBB. To verify whether BocBDP could cross the BBB, BocBDP was injected intravenously into a wild-type (WT) mouse and the fluorescence of the isolated brain was recorded. As shown in Fig. S4,† BocBDP crossed the BBB successfully and a bright red fluorescence signal was observed. APP/PS1 mice are a common animal model to generate Aβ in the brain.[43] We used an 18-month-old AD mouse (APP/PS1) and age-matched WT mouse for the following experiments. After intravenous injection of BocBDP (0.15 mg kg^{-1}), the fluorescence signals in the mouse brain were captured. As shown in Fig. 6a, both the WT mouse and APP/PS1 mouse exhibited higher fluorescence signals than the control group. The fluorescence intensities of the two types of mice increased gradually up until 60 minutes. Significantly, the signals in the brain region could be recorded continuously for more than 2 hours. We attributed the long imaging time to the hydrogen bonding interactions between Boc and amino acid residue K16. The hydrogen bonds of BocBDP seem to result in a longer metabolic processing time than for BAP-1. Notably, the fluorescence intensity in the brain regions of the APP/PS1 mouse was stable and constantly higher than the highest values observed for WT mice (Fig. 6b). The fluorescence intensity of the APP/PS1 mouse (at 60 minutes) was about 2 times higher than that of the WT mouse. BocBDP could specifically bind with Aβ plaques *in vivo*. The higher fluorescence signal in the APP/PS1 mouse was attributed to the strong interaction between BocBDP and Aβ plaques. Moreover, BocBDP could image Aβ plaques for at least 2 hours, which was longer than most previously reported probes.[30,44–47]

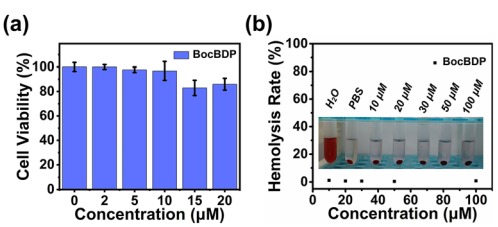

Fig. 5 Biocompatibility of BocBDP. (a) Cytotoxicity of BocBDP toward PC12 cells. (b) Hemolysis image and hemolysis rate of BocBDP with various concentrations. PBS and water were evaluated as controls.

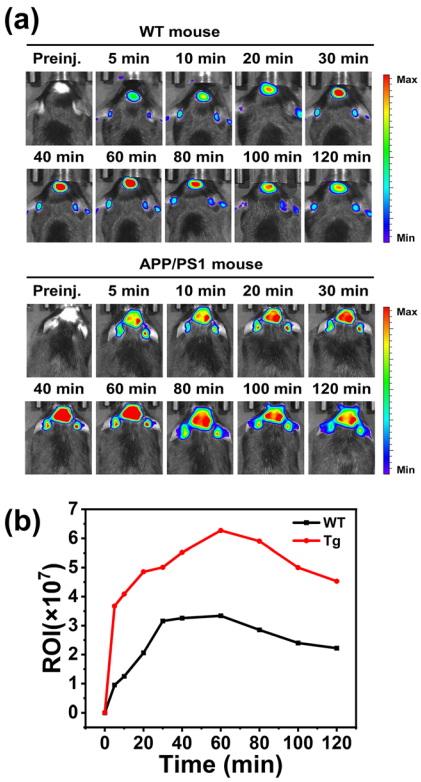

Fig. 6 *In vivo* fluorescence imaging in the brain region of the WT (C57BL/6J) mouse and APP/PS1 (C57BL/6J) mouse at different time points after intravenous injection of BocBDP (0.15 mg kg^{-1} in 20% 1,2-propanediol and 80% PBS). (a) The fluorescence signals of BocBDP between the WT mouse (top figure) and transgenic (T_g) mouse (bottom figure) at various time points. Preinj is before injection. (b) The relative fluorescence signal [(p s^{-1} cm^{-2} sr^{-1})/(μW cm^{-2})] in the brain regions of the WT mouse and T_g mouse at various time points.

Conclusions

In this research, we developed a new probe BocBDP for detecting and imaging Aβ plaques. BocBDP consists of a Aβ recognition unit [4-(Boc-amino) benzene] and a BODIPY fluorophore. BocBDP interacts with amino acid residues Lys16 (K16), Val18 (V18), and Glu22 (E22). The hydrogen bonding interaction between the carbonyl oxygen atom in the Boc unit and Lys16 contributed to the strong binding with Aβ and stable imaging for an extended period of time. BocBDP exhibited a five-fold fluorescence enhancement and a high affinity for

$A\beta_{1-42}$ aggregates (K_d = 67.8 ± 3.18 nM). The enhanced fluorescence was the result of the insertion of BocBDP into the hydrophobic cavity of the $A\beta_{1-42}$ aggregates, restricting the motion of BocBDP and enhancing the fluorescence. The high affinity enabled BocBDP to image brain slices and Aβ solutions with a high signal-to-noise ratio. BocBDP has satisfactory log *P* and MW which enables BocBDP to cross the BBB, enabling the imaging of Aβ plaques in AD mice for up to 2 hours. We anticipate that our Aβ binding unit will facilitate the design and development of improved probes for Aβ imaging.

Conflicts of interest

There are no conflicts to declare.

Acknowledgements

We are thankful for the support from the Beijing Natural Science Foundation (No. 7232342), the Natural Science Foundation of China (No. 82131430174 and 81961138011), the Academy of Medical Sciences Newton Advanced Fellowship (NAFR13\1015), the National Key Research and Development Program of China (2021YFC2101500), and the China Scholarship Council. TDJ wishes to thank the Royal Society for a Wolfson Research Merit Award and the Open Research Fund of the School of Chemistry and Chemical Engineering, Henan Normal University for support (2020ZD01).

References

1 L. Mucke, Alzheimer's disease, *Nature*, 2009, **461**, 895–897.
2 J. Hardy and G. Higgins, Alzheimer's disease: The amyloid cascade hypothesis, *Science*, 1992, **256**, 184–185.
3 J. Hardy, The amyloid hypothesis for Alzheimer's disease: a critical reappraisal, *J. Neurochem.*, 2009, **110**, 1129–1134.
4 M. Cui, M. Ono, H. Watanabe, H. Kimura, B. Liu and H. Saji, Smart near-infrared fluorescence probes with donor–acceptor structure for in vivo detection of β-amyloid deposits, *J. Am. Chem. Soc.*, 2014, **136**, 3388–3394.
5 R. Nelson, M. Sawaya, M. Balbirnie, A. Madsen, C. Piekel, R. Grothe and D. Esienberg, Structure of the cross-β spine of amyloid-like fibrils, *Nature*, 2005, **435**, 773–778.
6 D. M. Walsh and D. J. Selkoe, Aβ Oligomers - a decade of discovery, *J. Neurochem.*, 2007, **101**, 1172–1184.
7 T. Mohamed, A. Shakeri and P. N. Rao, Amyloid cascade in Alzheimer's disease: Recent advances in medicinal chemistry, *Eur. J. Med. Chem.*, 2016, **113**, 258–272.
8 W. Tang, W. Fan, J. Lau, L. Deng, Z. Shen and X. Chen, Emerging blood–brain-barrier-crossing nanotechnology for brain cancer theranostics, *Chem. Soc. Rev.*, 2019, **48**, 2967–3014.
9 S. Liebne, R. M. Dijkhuizen, Y. Reiss, K. H. Plate, D. Agalliu and G. Constantin, Functional morphology of the blood-brain barrier in health and disease, *Acta Neuropathol.*, 2018, **135**, 311–336.
10 Z. Yang, W. Gao, Y. Liu, N. Pang and X. Qi, Delivering siRNA and chemotherapeutic molecules across BBB and BTB for intracranial glioblastoma therapy, *Mol. Pharmaceutics*, 2017, **14**, 1012–1022.
11 W. M. Pardridge, The blood-brain barrier: bottleneck in brain drug development, *NeuroRx*, 2005, **2**, 3–14.
12 J. F. Poduslo, G. L. Curran, J. A. Peterson, D. J. McCormick, A. H. Fauq, M. A. Khan and T. M. Wengenack, Design and chemical synthesis of a magnetic resonance contrast agent with enhanced in vitro binding, high blood-brain barrier permeability, and in vivo targeting to Alzheimer's disease amyloid plaques, *Biochemistry*, 2004, **43**, 6064–6075.
13 H. Quigley, S. J. Colloby and J. T. O'Brien, PET imaging of brain amyloid in dementia: a review, *Int. J. Geriatr. Psychiatry*, 2011, **26**, 991–999.
14 M. C. Cui, Z. J. Li, R. K. Tang and B. L. Liu, Synthesis and evaluation of novel benzothiazole derivatives based on the bithiophene structure as potential radiotracers for β-amyloid plaques in Alzheimer's disease, *Bioorg. Med. Chem.*, 2010, **18**, 2777–2784.
15 D. Wu, J. C. Ryu, Y. W. Chung, D. Lee, J. H. Ryu, J. H. Yoon and J. Yoon, A far-red-emitting fluorescence probe for sensitive and selective detection of peroxynitrite in Live cells and tissues, *Anal. Chem.*, 2017, **89**, 10924–10931.
16 F. Zhang, X. Liang, W. Zhang, Y. L. Wang, H. Wang, Y. H. Mohammed, B. Song, R. Zhang and J. Yuan, A unique iridium(III) complex-based chemosensor for multi-signal detection and multi-channel imaging of hypochlorous acid in liver injury, *Biosens. Bioelectron.*, 2017, **87**, 1005–1011.
17 J. An, P. Verwilst, H. Aziz, J. Shin, S. Lim, I. Kim, Y. K. Kim and J. S. Kim, Picomolar-sensitive β-amyloid fibril fluorophores by tailoring the hydrophobicity of biannulated π-elongated dioxaborine-dyes, *Bioact. Mater.*, 2022, **13**, 239–248.
18 V. Sander, S. V. Patke, S. Sahu, C. L. Teoh, P. Peng, Y. T. Chang and A. J. Davidson, The small molecule probe PT-Yellow labels the renal proximal tubules in zebrafish, *Chem. Commun.*, 2015, **51**, 395–398.
19 X. Wu, W. Shi, X. Li and H. Ma, Recognition moieties of small molecular fluorescent probes for bioimaging of enzymes, *Acc. Chem. Res.*, 2019, **52**, 1892–1904.
20 A. Aliyan, N. P. Cook and A. A. Marti, Interrogating amyloid aggregates using fluorescent probes, *Chem. Rev.*, 2019, **119**, 11819–11856.
21 S. T. Selvan, R. Ravichandar, K. K. Ghosh, A. Mohan, P. Mahalakshmi, B. Gulyás and P. Padmanabhan, Coordination chemistry of ligands: Insights into the design of amyloid beta/tau-PET imaging probes and nanoparticles-based therapies for Alzheimer's disease, *Coord. Chem. Rev.*, 2021, **430**, 213695.
22 B. Xiong, Y. Wang, Y. Chen, S. Xing, Q. Liao, Y. Chen, Q. Li, W. Li and H. Sun, Strategies for structural modification of small molecules to improve blood–brain barrier penetration: a recent perspective, *J. Med. Chem.*, 2021, **64**, 13152–13173.

23 K. Rajasekhar, N. Narayanaswamy, N. A. Murugan, K. Viccaro, H. G. Lee, K. Shah and T. Govindaraju, Aβ plaque-selective NIR fluorescence probe to differentiate Alzheimer's disease from tauopathies, *Biosens. Bioelectron.*, 2017, **98**, 54–61.
24 C. Ran, X. Xu, S. B. Raymond, B. J. Ferrara, K. Neal, B. J. Bacskai, Z. Medarova and A. Moore, Design, synthesis, and testing of difluoroboron-derivatized curcumins as near-infrared probes for in vivo detection of amyloid-β deposits, *J. Am. Chem. Soc.*, 2009, **131**, 15257–15261.
25 X. Wang, C. Wang, H. N. Chan, I. Ashok, S. K. Krishnamoorthi, M. Li, H. W. Li and M. S. Wong, Amyloid-β oligomer targeted theranostic probes for in vivo NIR imaging and inhibition of self-aggregation and amyloid-β induced ROS generation, *Talanta*, 2021, **224**, 1218300.
26 L. Ma, S. Yang, Y. Ma, Y. Chen, Z. Wang, T. D. James, X. Wang and Z. Wang, Benzothiazolium derivative-capped silica nanocomposites for β-amyloid imaging in vivo, *Anal. Chem.*, 2021, **93**, 12617–12627.
27 M. Groenning, Binding mode of Thioflavin T and other molecular probes in the context of amyloid fibrils-current status, *J. Chem. Biol.*, 2010, **3**, 1–18.
28 W. Fu, C. Yan, Z. Guo, J. Zhang, H. Zhang, H. Tian and W. H. Zhu, Rational design of near-infrared aggregation-induced-emission-active probes: In situ mapping of amyloid-β plaques with ultrasensitivity and high-fidelity, *J. Am. Chem. Soc.*, 2019, **141**, 3171–3177.
29 X. Y. Liu, X. J. Wang, L. Shi, Y. H. Liu, L. Wang, K. Li, Q. Bu, X. B. Cen and X. Q. Yu, Rational design of quinoxalinone-based red-emitting probes for high-affinity and long-term visualizing amyloid-β in vivo, *Anal. Chem.*, 2022, **94**, 7665–7673.
30 M. Ono, H. Watanabe, H. Kimura and H. Saji, BODIPY-based molecular probe for imaging of cerebral β-amyloid plaques, *ACS Chem. Neurosci.*, 2012, **3**, 319–324.
31 D. Zhao, Y. Chen, Q. Liu, Y. F. Zhao and Y. M. Li, Exploring the binding mechanism of thioflavin-T to the β-amyloid peptide by blind docking method, *Sci. China: Chem.*, 2012, **55**, 112–117.
32 M. Biancalana and S. Koide, Molecular mechanism of Thioflavin-T binding to amyloid fibrils, *Biochim. Biophys. Acta*, 2010, **1804**, 1405–1412.
33 J. D. Chodera and D. L. Mobley, Entropy-Enthalpy Compensation: Role and Ramifications in Biomolecular Ligand Recognition and Design, *Annu. Rev. Biophys.*, 2013, **42**, 121–142.
34 V. Lafont, A. A. Armstrong, H. Ohtaka, Y. Kiso, L. M. Amzel and E. Freire, Compensating Enthalpic and Entropic Changes Hinder Binding Affinity Optimization, *Chem. Biol. Drug Des.*, 2007, **69**, 413–422.
35 D. Chen, N. Oezguen, P. Urvil, C. Ferguson and T. C. Savidge, Regulation of protein-ligand binding affinity by hydrogen bond pairing, *Sci. Adv.*, 2016, **2**, e1501240.
36 *Protein Science Encyclopedia*, 2008, vol. 15, 9783527610754.
37 G. B. Ferreira, M. V. Acosta and W. F. A. Junior, Hydrogen Bonds in Protein-Ligand Complexes, *Methods Mol. Biol.*, 2019, **2053**, 93–107.
38 T. Lu and F. Chen, Multiwfn: A multifunctional wavefunction analyzer, *J. Comput. Chem.*, 2012, **33**, 580–592.
39 M. T. Colvin, R. Silvers, Q. Z. Ni, T. V. Can, I. Sergeyev, M. Rosay and R. G. Griffin, Atomic resolution structure of monomorphic $A\beta_{42}$ amyloid fibrils, *J. Am. Chem. Soc.*, 2016, **138**, 9663–9674.
40 R. Kawai, M. Araki, M. Yoshimura, N. Kamiya, M. Ono, H. Saji and Y. Okuno, Core binding site of a Thioflavin-T-Derived imaging probe on amyloid β fibrils predicted by computational methods, *ACS Chem. Neurosci.*, 2018, **9**, 957–966.
41 Y. Zhang, Z. Li, W. Hu and Z. Liu, A mitochondrial-targeting near-infrared fluorescent probe for visualizing and monitoring viscosity in live cells and tissues, *Anal. Chem.*, 2019, **15**, 10302–10309.
42 E. L. Gelamo, C. H. Silva, H. Imasato and M. Tabak, Interaction of bovine (BSA) and human (HSA) serum albumins with ionic surfactants: spectroscopy and modelling, *Biochim. Biophys. Acta*, 2002, **31**, 84–99.
43 K. Lok, H. Zhao, H. Shen, Z. Wang, X. Gao, W. Zhao and M. Yin, Characterization of the APP/PS1 mouse model of Alzheimer's disease in senescence accelerated background, *Neurosci. Lett.*, 2013, **557**, 84–89.
44 H. Watanabe, M. Ono, K. Matsumura, M. Yoshimura, H. Kimura and H. Saji, Molecular imaging of β-Amyloid plaques with near-infrared boron dipyrromethane (BODIPY)-based fluorescent probes, *Mol. Imaging*, 2013, **12**, 5.
45 X. Zhang, Y. Tian, C. Zhang, X. Tian, A. W. Ross, R. D. Moir, H. Sun, R. E. Tanzi and C. Ran, Near-infrared fluorescence molecular imaging of amyloid beta species and monitoring therapy in animal models of Alzheimer's disease, *Proc. Natl. Acad. Sci. U. S. A.*, 2015, **112**, 9734–9739.
46 Y. Cheng, B. Zhu, X. Li, G. Li, S. Yang and Z. Zhang, A pyrane based fluorescence probe for noninvasive prediction of cerebral β-amyloid fibrils, *Bioorg. Med. Chem. Lett.*, 2015, **25**, 4472–4476.
47 H. Yang, J. Zhang, Y. Zang, H. Zhang, J. Li, G. Chen and X. He, D-A-D fluorogenic probe for the rapid imaging of amyloid β plaques in vivo, *Dyes Pigm.*, 2017, **136**, 224–228.